

Phase locking and fractional Shapiro steps in collective dynamics of microparticles

Seemant Mishra,^{1,*} Artem Ryabov,^{2,†} and Philipp Maass^{1,‡}

¹*Universität Osnabrück, Fachbereich Mathematik/Informatik/Physik, BarbarasträÙe 7, D-49076 Osnabrück, Germany*

²*Charles University, Faculty of Mathematics and Physics,*

Department of Macromolecular Physics, V Holešovičkách 2, CZ-18000 Praha 8, Czech Republic

(Dated: December 19, 2024)

In driven nonlinear systems, phase locking is an intriguing effect leading to robust stationary states that are stable over extended ranges of control parameters. Recent experiments allow for exploring microscopic mechanisms underlying such phenomena in collective dynamics of micro- and nanoparticles. Here we show that phase-locked dynamics of hardcore-interacting microparticles in a densely populated periodic potential under time-periodic driving arises from running solitary cluster waves. We explain how values of phase-locked currents are related to soliton velocities and why collective particle dynamics synchronize with the driving for certain particle diameters only. Our analysis is based on an effective potential for the solitary wave propagation and a unit displacement law, saying that the total average shift of all particle positions per soliton period equals one wavelength of the periodic potential.

Phase locking is a fundamental phenomenon in periodically driven systems with nonlinear dynamics [1]. A prominent example are steps in the current-voltage characteristics of Josephson junctions driven by radio-frequency fields, commonly known as Shapiro steps [2, 3]. Generally, these steps emerge when a system settles into a robust stationary limit cycle, which is stable against changes of one or more of its control parameters. Analogous phase-locking effects were found in a large variety of nonlinear systems like superconducting nanowires [4–6], charge density waves [7–11], skyrmions [12–16], vortex lattices [17–19], as well as in colloidal systems for both single-particle [20, 21] and collective dynamics [20, 22–28].

For single-particle dynamics in a periodic potential $U(x)$ with wavelength λ under time-periodic driving $F(t)$ with period τ , phase-locked stationary states are synchronized with the driving, i.e. have a period equal to an integer multiple $q\tau$ of τ , $q \in \mathbb{N}$. For the particle to move between equivalent points of $U(x)$ in the period $q\tau$, the distance between those points must be an integer multiple $p\lambda$ of λ , $p \in \mathbb{N}$. In such a state, the particle moves with mean velocity v having the phase-locked value

$$v_{p,q} = \frac{p}{q} \frac{\lambda}{\tau}. \quad (1)$$

The stationary state is often robust against small changes of control parameters, causing a mode with velocity $v_{p,q}$ to appear over a certain range of e.g. amplitudes or frequencies of the time-periodic driving. Which p/q occur depends on the type of microscopic dynamics, driving, and shape of the periodic potential. For overdamped motion in a sinusoidal potential, in particular, only integer multiples of λ/τ are robust phase-locked velocities

[29].

For many-particle dynamics, phase locking is less well understood and often puzzling. Here we explain how it arises in collective dynamics of microparticles due to motion of solitary cluster waves. These waves enable particle transport over potential barriers even if the barriers are orders of magnitudes higher than the thermal energy $k_B T$ [30, 31].

Specifically, we consider overdamped Brownian motion of N microparticles with hardcore interactions in L/λ periods of a densely populated sinusoidal potential $U(x) = (U_0/2) \cos(2\pi x/\lambda)$ with barriers $U_0 \gg k_B T$ subject to periodic boundary conditions. The particles are driven by a time-periodic force $F(t) = F_{dc} + F_{ac} \sin(2\pi t/\tau)$, see the illustration in Fig. 1. Their collective motion is explored by Brownian dynamics simulations. Underlying Langevin equations are detailed in Supplemental material (SM), including methods how to solve them numerically and to determine relevant quantities, see below.

Collective particle dynamics in the stationary state of this system shows phase locking behavior with remarkable features, as reflected in time-averaged currents shown in Fig. 2:

(i) Although we are confronted with complex many-

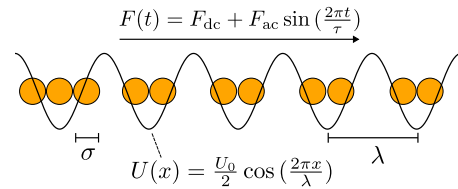


FIG. 1. Microparticles with hard-sphere diameter σ moving in a sinusoidal potential $U(x)$ with wavelength λ and potential barrier U_0 . The particles perform an overdamped Brownian motion in a fluidic environment with temperature T and are driven by a time-periodic force $F(t)$. We use λ , U_0 and $\lambda^2/\mu U_0$ as units of length, energy and time, where μ is the particle mobility.

* semishra@uos.de

† rjabov.a@gmail.com

‡ maass@uos.de

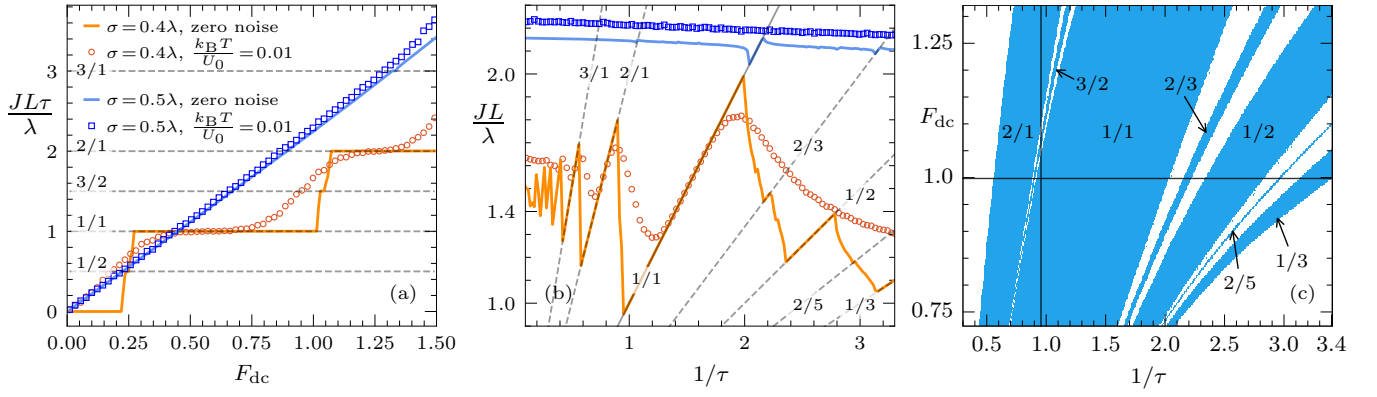


FIG. 2. Scaled stationary particle currents J for the system shown in Fig. 1 reflecting phase-locked dynamics. In (a), simulated currents are plotted as a function of the constant drag force F_{dc} at fixed $F_{ac} = 1.5$ and $1/\tau = 3/\pi$. They show Shapiro steps at phase-locked values $J_{p,q}$ [Eq. (2)]. In (b), simulated currents are plotted as a function of the driving frequency $1/\tau$ at fixed $F_{dc} = 1$ and $F_{ac} = 1.5$ and the phase locked values $J_{p,q}$ show up as constant slopes in different intervals of $1/\tau$. Data are shown for a system with $L/\lambda = 20$ potential wells and $N = 21$ particles for two hard-sphere diameters $\sigma = 0.4\lambda$ and $\sigma = 0.5\lambda$ in the zero-noise limit ($k_B T/U_0 \rightarrow 0$) and for a finite temperature, $k_B T/U_0 = 0.01$ [legend in (a) applies also to panel (b)]. The currents in (a) and (b) are scaled with $L\tau/\lambda$ and L/λ , by which steps in (a) and slopes in (b) have rational values p/q , see Eq. (2). (c) Diagram of phase locked currents $J_{p,q}$ for $\sigma = 0.4\lambda$ in dependence of $1/\tau$ and F_{dc} for fixed $F_{ac} = 1.5$. The diagram was calculated from Eqs. (S18), (S19) in SM. Following the vertical and horizontal lines in the diagram yields the modes $J_{p,q}$ obtained in (a) and (b).

particle dynamics, the phase-locked currents $J_{p,q}$ have values as if a single particle would be driven by a time-periodic force in a periodic potential with L/λ periods of wavelength λ , i.e. with $\rho = 1/L$ and $v_{p,q} = p\lambda/q\tau$:

$$J_{p,q} = \rho v_{p,q} = \frac{p}{q} \frac{\lambda}{L\tau}. \quad (2)$$

- (ii) Despite the potential being sinusoidal, fractional $J_{p,q}$ occur, with p not divisible by q in Eq. (2).
- (iii) Occurrence of phase locking depends sensitively on the particle diameter σ : for certain σ , pronounced Shapiro steps appear ($\sigma = 0.4\lambda$ in Fig. 2), while they are nearly absent for other σ ($\sigma = 0.5\lambda$ in Fig. 2).

Ideal sharp Shapiro steps are obtained in the limit of zero noise ($k_B T/U_0 \rightarrow 0$). Pronounced ones can be clearly visible also for temperatures well accessible in experiments [31, 32], see the curves for $k_B T/U_0 = 10^{-2}$ in Fig. 2.

We show that the puzzling features (i)-(iii) in the many-particle dynamics originate from an effective potential for solitary wave propagation and a law for the sum of all particle displacements in one wave period.

Solitary cluster waves, in short cluster solitons, were recently predicted for overdamped Brownian motion under a constant drag force [30] and shortly after confirmed in experiments [31]. They characterize running states when wells of a periodic potential are filled by particles beyond a limit, where a mechanically stable state ceases to exist.

The solitons turn out to mediate particle transport also under additional time-periodic driving. Figure 3 illustrates a propagation in the zero-noise limit, where clusters of particles in contact form. Most of the clusters in

Fig. 3 consist of three particles (red). We call them basic stable clusters, because in the absence of time-periodic driving ($F_{ac} = 0$), they build up a stable configuration with largest particle number [33]. For $F_{ac} > 0$, these basic clusters of size $n_b = 3$ perform localized oscillatory motions.

In addition, we see a 2-cluster (orange), which at a time t_{det} is formed by detachment from a 3-cluster (green). Shortly before the detachment, the 3- and 2-clusters

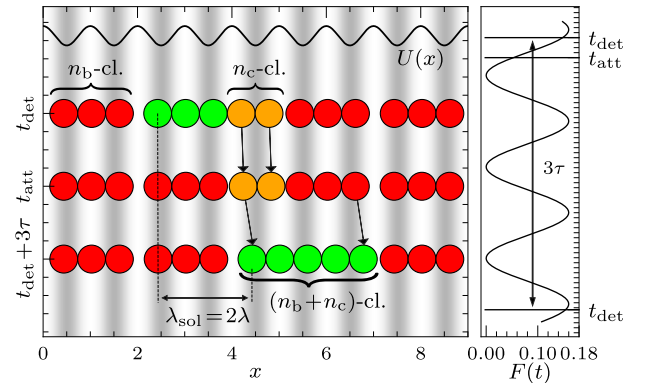


FIG. 3. Simulated particle configurations in a phase-locked steady state at different times for a soliton-carrying section of a system with $L/\lambda = 23$ potential wells and $N = 35$ particles of size $\sigma = 0.59\lambda$. White and grey shaded stripes represent regions close to maxima and minima of the sinusoidal potential $U(x)$ (solid line at top of graph), respectively. Parameters of the time-periodic forcing $F(t)$, shown on the right side, are $F_{dc} = F_{ac} = 0.08$ and $\tau = 0.875$. For meaning of labelings (time, colored particle clusters, distances), see main text.

formed a 5-cluster. After a slight movement of the 2-cluster, it attaches to a 3-cluster at time t_{att} . The resulting 5-cluster moves over a long time interval until time $t_{\text{det}} + 3\tau$. The configuration at this time instant corresponds to that in the first row, at time t_{det} , i.e. at an infinitesimal time later, a 2-cluster detaches and the whole process repeats itself. The sequential creation of slightly moving 2- and 5-clusters propagates as a solitary wave. Its propagation is demonstrated in the video of SM.

In the example above, the 2-cluster represents the core soliton cluster of size $n_c = 2$ and the 5-cluster the composite soliton cluster of size $n_b + n_c = 5$. We define the instantaneous position of the soliton by the position of the leftmost particle in a soliton cluster, i.e. the core or composite cluster. The soliton motion is periodic in space with period λ_{sol} . Phase locking between soliton propagation and oscillatory force manifests itself in that the soliton moves p periods λ_{sol} in q time periods τ of the oscillatory force, implying phase-locked values $(p/q)\lambda_{\text{sol}}/\tau$ for the mean soliton velocity v_{sol} . This fact is demonstrated in Fig. 4(c) (orange line), where v_{sol} is shown as a function of $\lambda_{\text{sol}}/\tau$ for the parameters in Fig. 3 ($p = 1$, $\lambda_{\text{sol}} = 2\lambda$, and $q = 3$).

The relation between solitary wave and particle dynamics enables us to understand the phase locking in the many-particle system by considering an effective local soliton potential $U_{\text{sol}}(x)$, the wavelength λ_{sol} of the solitary wave, and a unit particle displacement law per soliton period.

The soliton potential gives the time-averaged mean force acting on the core and composite soliton cluster ($F_{\text{ac}} = 0$). It is

$$U_{\text{sol}}(x) = \begin{cases} U_{n_c}(x) + C, & \text{core cluster at } x, \\ U_{n_b+n_c}(x), & \text{composite cluster at } x, \end{cases} \quad (3)$$

where $U_n(x) = \sum_{i=0}^{n-1} U(x + i\sigma)/n$. The constant $C = U_{n_b+n_c}(x_{\text{att}}) - U_{n_c}(x_{\text{att}})$ is added to make $U_{\text{sol}}(x)$ continuous at $x = x_{\text{att}}$. The range of positions x in Eq. (3) covers the interval $[x_{\text{det}}^+, x_{\text{det}}^-]$, where x_{det}^+ is the soliton position right after the detachment of the core n_c -cluster from the composite $(n_b + n_c)$ -cluster. The distance $x_{\text{det}}^- - x_{\text{det}}^+$ is smaller than λ and equals the empty gap between two successive n_b clusters. For the parameters in Fig. 3, $U_{\text{sol}}(x)$ is displayed in Fig. 4(a).

Given $U_{\text{sol}}(x)$, one can map the soliton dynamics onto that of a single quasiparticle moving in a potential $U_{\text{sp}}(x)$ obtained by stitching together copies of $U_{\text{sol}}(x)$, see the inset of Fig. 4(a). Remarkably, $U_{\text{sp}}(x)$ has an inherent tilt, since $U_{\text{sol}}(x_{\text{det}}^+)$ and $U_{\text{sol}}(x_{\text{det}}^-)$ are different for $F_{\text{dc}} > 0$. Without the tilt, the single-particle potential is periodic with wavelength $\lambda_{\text{sp}} = x_{\text{det}}^- - x_{\text{det}}^+$.

Based on this periodic potential, we can understand the occurrence of fractional Shapiro steps and the strong sensitivity of the phase locking on the particle size. Fractional Shapiro steps can occur, because the periodic potential is not sinusoidal. The strong sensitivity arises

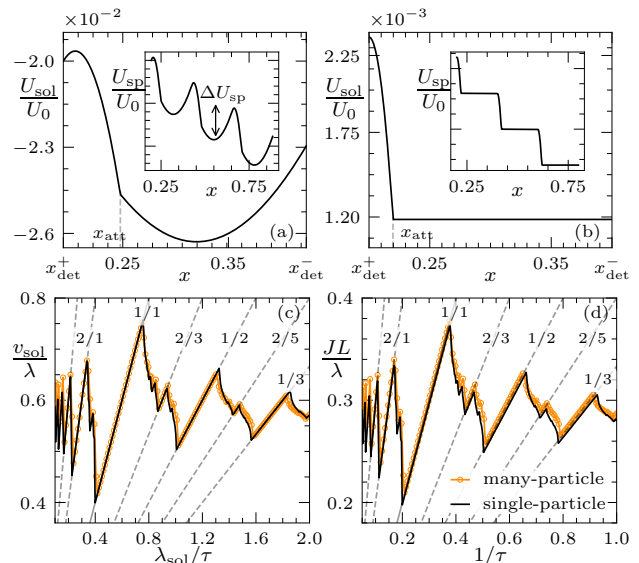


FIG. 4. (a) Soliton potential $U_{\text{sol}}(x)$ [Eq. (3)] for parameters as in Fig. 3 ($\sigma = 0.59\lambda$). It is shown for one period $\lambda_{\text{sp}} = x_{\text{det}}^- - x_{\text{det}}^+$ corresponding to one period λ_{sol} of the soliton motion. At x_{att} it has a cusp because the propagating soliton cluster changes from the core to the composite cluster. The inset shows three periods of the single-particle potential $U_{\text{sp}}(x)$ with barrier ΔU_{sp} , obtained by stitching copies of $U_{\text{sol}}(x)$. (b) Soliton potential $U_{\text{sol}}(x)$ and barrier-free single-particle potential $U_{\text{sp}}(x)$ (inset) for $\sigma = 0.6\lambda$. (c), (d) Mean soliton velocity v_{sol} (symbols) as a function of $\lambda_{\text{sol}}/\tau$ and mean particle current J (multiplied by L/λ) as a function of $1/\tau$ for $\sigma = 0.59\lambda$. The simulated data show many linear segments with indicated rational slopes p/q . Solid black lines were calculated from trajectories of a single particle moving in $U_{\text{sp}}(x)$ and driven by $F(t)$. In (c), single-particle velocities were scaled by $\lambda_{\text{sol}}/\lambda_{\text{sp}}$, and in (d) currents were obtained by weighting of instantaneous velocities and time-averaging described in the main text.

since even a small change of σ can alter the shape of $U_{\text{sp}}(x)$ from one exhibiting barriers ΔU_{sp} to one without barriers, and barriers are necessary to obtain perceptible phase locking [34]. For example, $U_{\text{sp}}(x)$ in Fig. 4(a) for $\sigma = 0.59\lambda$ has barriers, while it has no barriers for $\sigma = 0.6\lambda$, see insets of Figs. 4(a), (b). Likewise, for $\sigma = 0.4\lambda$ in Fig. 2, $U_{\text{sp}}(x)$ has barriers, and no ones for $\sigma = 0.5\lambda$, see SM.

By generating trajectories of single-particle motion in the force field $F(t) - dU_{\text{sp}}/dx$ as described in SM, we can moreover obtain v_{sol} and J in the many-particle system with high accuracy after following transformations.

The velocity v_{sol} is obtained by rescaling the mean single-particle velocity v_{sp} . In one period λ_{sp} of the single-particle motion, the associated soliton moves a distance $\lambda_{\text{sol}} > \lambda_{\text{sp}}$. This is because one needs to take into account the jumps $(\lambda_{\text{sol}} - \lambda_{\text{sp}})$ occurring in soliton trajectories at detachment events. Hence, $v_{\text{sol}} = (\lambda_{\text{sol}}/\lambda_{\text{sp}})v_{\text{sp}}$.

For calculating λ_{sol} , we consider two successive points

where a core cluster attaches to a basic cluster. The distance between the first particles of the two basic clusters in the attachment events have distance $\lceil n_b(\sigma/\lambda) \rceil \lambda$, where $\lceil x \rceil$ is the smallest integer larger than x . Hence,

$$\lambda_{\text{sol}} = \left\lceil n_b \frac{\sigma}{\lambda} \right\rceil \lambda. \quad (4)$$

For $n_b = 3$ and $\sigma = 0.59\lambda$ in Fig. 3, $\lceil n_b(\sigma/\lambda) \rceil = 2$, see the spacing between the dotted lines. Rescaled single-particle velocities are in excellent agreement with v_{sol} in the many-particle system, see the black solid line in Fig. 4(c).

From the phase-locked soliton velocities $v_{p,q} = (p/q)\lambda_{\text{sol}}/\tau$ and the single-particle picture one may expect that $J_{p,q} = v_{p,q}/L$ gives the phase-locked many-particle currents. However, the current in Fig. 4(d) does not display values $LJ_{p,q}/\lambda = (p/q)2/\tau$ for $\lambda_{\text{sol}} = 2\lambda$, but we obtain by a factor 1/2 smaller values $LJ_{p,q}/\lambda = (p/q)/\tau$, i.e. $J_{p,q} = v_{p,q}/2L$. Thus, the naive picture of a soliton as a current carrying quasiparticle does not apply.

To obtain the currents from single-particle trajectories, one needs to include a weighting factor $n(x)$ accounting for the fact that n_c (or $n_b + n_c$) particles are moving in the many-particle system if the single particle is at a position x of a core (or composite) soliton cluster. Then, J is obtained by time-averaging $n(x_{\text{sp}}(t))v_{\text{sp}}(t)/L$, where $x_{\text{sp}}(t)$ and $v_{\text{sp}}(t)$ are the position and velocity of the single particle at time t . The so-calculated currents, shown as black solid line in Fig. 4(d), reproduce very well the many-particle currents.

The weighting of single-particle velocities gives insight why $J_{p,q}$ differs from $v_{p,q}/L$, but it does not explain why $J_{p,q} = v_{p,q}/2L$. This relation follows from the fact that the sum of all N particle displacements is $p\lambda$ if the soliton moves p wavelengths λ_{sol} , i.e. a unit displacement law holds on average:

$$\frac{1}{p} \left[\sum_{i=1}^N \Delta x_i \right]_{p \text{ soliton}} = \lambda. \quad (5)$$

Accordingly, for the p/q -phase locked soliton motion, the phase-locked values of the particle current is $J_{p,q} = (1/L) \sum_{i=1}^N \Delta x_i / q\tau = (p/q)\lambda/L\tau = v_{p,q}/2L$. That is, the factor 1/2 follows from the fact that the soliton moves λ_{sol} in one period of the driving, while the mean total displacement of all particles per soliton period is $\lambda = \lambda_{\text{sol}}/2$.

Using $U_{\text{sp}}(x)$, we can also predict the intervals of driving parameters where phase-locked modes with certain p and q occur in the limit of zero noise. The procedure is described in SM and demonstrated by a diagram of phase-locked modes in Fig. 2(c). When following the horizontal and vertical lines in the diagram, we can infer the phase-locked current modes shown in Figs. 2(a),(b). For example, the modes with $p/q = 2/1, 1/1$, and $1/2$ appear for $1/\tau$ in the intervals 0.56-0.87, 0.92-2.03, and 2.33-2.80 in Fig. 2(c), which is in excellent agreement with the corresponding intervals of $1/\tau$ in Fig. 2(b).

Let us now discuss the impact of thermal noise on the phase locking that is rather strong in general [35–37]. Its disturbing influence is the smaller the larger $\Delta U_{\text{sp}}/k_{\text{B}}T$. Studies of Josephson junctions show that phase locking can be destroyed for thermal energies much less than the barrier of the periodic potential [34]. For the system in Fig. 2 we calculated $\Delta U_{\text{sp}}/U_0$ as a function of σ , see SM. The ΔU_{sp} are much smaller than U_0 and run through maxima between zero points occurring at diameters $\sigma = (n-1)/n\lambda$, $n = 2, 3, \dots$ [30]. Overall, the barriers $\Delta U_{\text{sp}}/k_{\text{B}}T$ decrease with σ , making small diameters favorable for studies of phase-locking in the many-particle system at finite thermal noise. For $\sigma = 0.4\lambda$, barriers ΔU_{sp} are about $0.18U_0$ and the phase locking is well visible for $k_{\text{B}}T = 0.01U_0$.

In summary, we have shown how phase-locked dynamics arise for microparticles driven by a time-periodic force with frequency $1/\tau$ through a densely populated sinusoidal potential in a fluidic environment. Responsible are phase-locked dynamics of solitary cluster waves with a wavelength λ_{sol} that is an integer multiple of the wavelength λ of the sinusoidal potential. To describe the wave propagation, we have constructed an effective periodic potential for the time-averaged soliton motion. This potential is nonsinusoidal, leading to fractional phase-locked values $(p/q)\lambda_{\text{sol}}/\tau$ of the mean soliton velocity ($p, q \in \mathbb{N}$). It allows one to determine diagrams of phase-locked modes and to estimate temperature limits, where phase-locking in the many-particle system becomes destroyed by thermal noise.

The solitary cluster waves mediate particle displacements, leading to fractional phase-locked current values in the many-particle system. A total sum of particle displacements $p\lambda$ is generated if a soliton travels p periods λ_{sol} . This corresponds to a remarkable unit displacement law: per period λ_{sol} on average, the sum of particle displacements is λ . As a consequence, particle currents in the many-particle systems exhibit phase-locked values $(p/q)\lambda/\tau$ equal to those of a single driven particle in the periodic potential.

The phase-locking is well observable in the presence of thermal noise, and Shapiro steps can remain clearly visible at ambient temperatures in experiments with colloidal particles [20, 21, 31, 38]. In these experiments, possible imperfections need to be considered also, as, e.g., a weak amplitude modulation of the periodic optical potential and small polydispersity. We have checked that the phase locking effects shown in Figs. 2(a),(b) are robust against such imperfections.

For larger system sizes or larger particle numbers, it is possible that several solitons are propagating [31, 33]. In such cases, we conjecture that the unit displacement law applies per soliton, giving phase-locked currents $J_{p,q} = (p/q)N_{\text{sol}}\lambda/\tau$, where N_{sol} is the number of solitons.

Analogous synchronized solitary wave propagation are expected to occur for other periodic potentials and repulsive particle interactions. An open question is what types of mechanisms lead to phase-locking of many-particle

currents in underdamped Brownian dynamics.

Our theoretical approach can be useful for interpreting experiments. This includes already existing observations, as the phase-locked kink dynamics in a chain of magnetically interacting particles [20]. It was associated with a density wave, which resembles the solitary cluster wave considered here. Extended regimes of constant phase-locked particle currents as a function of the driving amplitude have been observed in driven motion of superparamagnetic particles across a magnetic bubble lattice [22, 23], and in molecular dynamics simulations [39] modelling experiments on particle transport across colloidal monolayers [24, 25, 27, 28]. Detailed information on individual particle motions accessible in such experiments can be utilized to test and extend the concepts of an effective potential for cluster solitons and the unit

displacement law for connecting solitary wave motion to many-particle transport.

ACKNOWLEDGMENTS

We thank A. Antonov and S. Schweers for their work on code development, and P. Tierno for very helpful discussions on soliton dynamics in experiments. We gratefully acknowledge financial support by the Czech Science Foundation (Project No. 23-09074L) and the Deutsche Forschungsgemeinschaft (Project No. 521001072), and the use of a high-performance computing cluster funded by the Deutsche Forschungsgemeinschaft (Project No. 456666331).

-
- [1] A. Pikovsky, M. Rosenblum, and J. Kurths, *Synchronization: A Universal Concept in Nonlinear Sciences*, Cambridge Nonlinear Science Series (Cambridge University Press, Cambridge, 2001).
- [2] B. D. Josephson, Possible new effects in superconductive tunnelling, *Phys. Lett.* **1**, 251 (1962).
- [3] S. Shapiro, Josephson currents in superconducting tunneling: The effect of microwaves and other observations, *Phys. Rev. Lett.* **11**, 80 (1963).
- [4] I. Dinsmore, R. C., M.-H. Bae, and A. Bezryadin, Fractional order Shapiro steps in superconducting nanowires, *Appl. Phys. Lett.* **93**, 192505 (2008).
- [5] M.-H. Bae, R. C. I. Dinsmore, T. Aref, M. Brenner, and A. Bezryadin, Current-phase relationship, thermal and quantum phase slips in superconducting nanowires made on a scaffold created using adhesive tape, *Nano Lett.* **9**, 1889 (2009).
- [6] J. Ridderbos, M. Brauns, A. Li, E. P. A. M. Bakkers, A. Brinkman, W. G. van der Wiel, and F. A. Zwanenburg, Multiple Andreev reflections and Shapiro steps in a Ge-Si nanowire Josephson junction, *Phys. Rev. Mater.* **3**, 084803 (2019).
- [7] G. Grüner and A. Zettl, Charge density wave conduction: A novel collective transport phenomenon in solids, *Phys. Rep.* **119**, 117 (1985).
- [8] G. Grüner, The dynamics of charge-density waves, *Rev. Mod. Phys.* **60**, 1129 (1988).
- [9] R. E. Thorne, J. S. Hubacek, W. G. Lyons, J. W. Lyding, and J. R. Tucker, ac-dc interference, complete mode locking, and origin of coherent oscillations in sliding charge-density-wave systems, *Phys. Rev. B* **37**, 10055 (1988).
- [10] M. F. Hundley and A. Zettl, Noise and ac-dc interference phenomena in the charge-density-wave conductor $K_{0.3}MoO_3$, *Phys. Rev. B* **39**, 3026 (1989).
- [11] A. A. Sinchenko and P. Monceau, Dynamical transport properties of $NbSe_3$ with simultaneous sliding of both charge-density waves, *Phys. Rev. B* **87**, 045105 (2013).
- [12] C. Reichhardt and C. J. O. Reichhardt, Shapiro steps for skyrmion motion on a washboard potential with longitudinal and transverse ac drives, *Phys. Rev. B* **92**, 224432 (2015).
- [13] C. Reichhardt and C. J. O. Reichhardt, Shapiro spikes and negative mobility for skyrmion motion on quasi-one-dimensional periodic substrates, *Phys. Rev. B* **95**, 014412 (2017).
- [14] T. Sato, A. Kikkawa, Y. Taguchi, Y. Tokura, and F. Kagawa, Mode locking phenomena of the current-induced skyrmion-lattice motion in microfabricated MnSi, *Phys. Rev. B* **102**, 180411 (2020).
- [15] N. P. Vizirim, C. J. O. Reichhardt, P. A. Venegas, and C. Reichhardt, Skyrmion dynamics and transverse mobility: skyrmion hall angle reversal on 2d periodic substrates with dc and biharmonic ac drives, *Eur. Phys. J. B* **93**, 112 (2020).
- [16] J. C. B. Souza, N. P. Vizirim, C. J. O. Reichhardt, C. Reichhardt, and P. A. Venegas, Shapiro steps and stability of skyrmions interacting with alternating anisotropy under the influence of ac and dc drives, *Phys. Rev. B* **110**, 014406 (2024).
- [17] C. Reichhardt, R. T. Scalettar, G. T. Zimányi, and N. Grønbech-Jensen, Phase-locking of vortex lattices interacting with periodic pinning, *Phys. Rev. B* **61**, R11914 (2000).
- [18] C. Reichhardt and F. Nori, Phase locking, devil's staircases, Farey trees, and Arnold tongues in driven vortex lattices with periodic pinning, *Phys. Rev. Lett.* **82**, 414 (1999).
- [19] A. B. Kolton, D. Domínguez, and N. Grønbech-Jensen, Mode locking in ac-driven vortex lattices with random pinning, *Phys. Rev. Lett.* **86**, 4112 (2001).
- [20] M. P. N. Juniper, A. V. Straube, R. Besseling, D. G. A. L. Aarts, and R. P. A. Dullens, Microscopic dynamics of synchronization in driven colloids, *Nat. Commun.* **6**, 7187 (2015).
- [21] M. P. N. Juniper, U. Zimmermann, A. V. Straube, R. Besseling, D. G. A. L. Aarts, H. Löwen, and R. P. A. Dullens, Dynamic mode locking in a driven colloidal system: experiments and theory, *New J. Phys.* **19**, 013010 (2017).
- [22] P. Tierno and T. M. Fischer, Excluded volume causes integer and fractional plateaus in colloidal ratchet currents, *Phys. Rev. Lett.* **112**, 048302 (2014).
- [23] P. Tierno, T. H. Johansen, and T. M. Fischer, Fast and rewritable colloidal assembly via field synchronized par-

- ticle swapping, *Appl. Phys. Lett.* **104**, 174102 (2014).
- [24] T. Bohlein, J. Mikhael, and C. Bechinger, Observation of kinks and antikinks in colloidal monolayers driven across ordered surfaces, *Nat. Mater.* **11**, 126 (2012).
- [25] T. Bohlein and C. Bechinger, Experimental observation of directional locking and dynamical ordering of colloidal monolayers driven across quasiperiodic substrates, *Phys. Rev. Lett.* **109**, 058301 (2012).
- [26] T. Brazda, C. Joly, and C. Bechinger, Experimental observation of Shapiro-steps in colloidal monolayers driven across time-dependent substrate potentials, *Soft Matter* **13**, 4024 (2017).
- [27] T. Brazda, A. Silva, N. Manini, A. Vanossi, R. Guerra, E. Tosatti, and C. Bechinger, Experimental observation of the Aubry transition in two-dimensional colloidal monolayers, *Phys. Rev. X* **8**, 011050 (2018).
- [28] A. Vanossi, C. Bechinger, and M. Urbakh, Structural lubricity in soft and hard matter systems, *Nat. Commun.* **11**, 4657 (2020).
- [29] J. R. Waldram and P. H. Wu, An alternative analysis of the nonlinear equations of the current-driven Josephson junction, *J. Low Temp. Phys.* **47**, 363 (1982).
- [30] A. P. Antonov, A. Ryabov, and P. Maass, Solitons in overdamped Brownian dynamics, *Phys. Rev. Lett.* **129**, 080601 (2022).
- [31] E. Cereceda-López, A. P. Antonov, A. Ryabov, P. Maass, and P. Tierno, Overcrowding induces fast colloidal solitons in a slowly rotating potential landscape, *Nat. Commun.* **14**, 6448 (2023).
- [32] E. Cereceda-López, D. Lips, A. Ortiz-Ambriz, A. Ryabov, P. Maass, and P. Tierno, Hydrodynamic interactions can induce jamming in flow-driven systems, *Phys. Rev. Lett.* **127**, 214501 (2021).
- [33] A. P. Antonov, A. Ryabov, and P. Maass, Solitary cluster waves in periodic potentials: Formation, propagation, and soliton-mediated particle transport, *Chaos, Solitons & Fractals* **185**, 115079 (2024).
- [34] R. L. Kautz, Noise, chaos, and the Josephson voltage standard, *Rep. Prog. Phys.* **59**, 935 (1996).
- [35] J. Tekić and B. Hu, Noise-induced Bessel-like oscillations of Shapiro steps with the period of the ac force, *Phys. Rev. B* **78**, 104305 (2008).
- [36] P. Mali, J. Tekić, Z. Ivić, and M. Pantić, Effects of noise on interference phenomena in the presence of subharmonic Shapiro steps, *Phys. Rev. E* **86**, 046209 (2012).
- [37] P. Mali, A. Šakota, J. Tekić, S. Radošević, M. Pantić, and M. Pavkov-Hrvojević, Complexity of Shapiro steps, *Phys. Rev. E* **101**, 032203 (2020).
- [38] M. P. N. Juniper, A. V. Straube, D. G. A. L. Aarts, and R. P. A. Dullens, Colloidal particles driven across periodic optical-potential-energy landscapes, *Phys. Rev. E* **93**, 012608 (2016).
- [39] S. V. Paronuzzi Ticco, G. Fornasier, N. Manini, G. E. Santoro, E. Tosatti, and A. Vanossi, Subharmonic Shapiro steps of sliding colloidal monolayers in optical lattices, *J. Phys. Condens. Matter* **28**, 134006 (2016).
- [40] A. P. Antonov, S. Schweers, A. Ryabov, and P. Maass, Brownian dynamics simulations of hard rods in external fields and with contact interactions, *Phys. Rev. E* **106**, 054606 (2022).
- [41] A. P. Antonov, S. Schweers, A. Ryabov, and P. Maass, Fast brownian cluster dynamics, *Comput. Phys. Commun.* **309**, 109474 (2025).
- [42] P. Strating, Brownian dynamics simulation of a hard-sphere suspension, *Phys. Rev. E* **59**, 2175 (1999).
- [43] A. Scala, Event-driven Langevin simulations of hard spheres, *Phys. Rev. E* **86**, 026709 (2012).
- [44] S. H. Strogatz, *Nonlinear Dynamics and Chaos: With Applications to Physics, Biology, Chemistry, and Engineering (2nd ed.)* (CRC Press, Boca Raton, 2015).
- [45] W. H. Press, S. A. Teukolsky, W. T. Vetterling, and B. P. Flannery, *Numerical recipes in C: the art of scientific computing*, 3rd ed. (Cambridge University Press, Cambridge, UK, 2007).

Supplemental Material for

Phase locking and fractional Shapiro steps in collective dynamics of microparticles

Seemant Mishra,¹ Artem Ryabov,² and Philipp Maass¹

¹*Universität Osnabrück, Fachbereich Mathematik/Informatik/Physik,
Barbarastraße 7, D-49076 Osnabrück, Germany*

²*Charles University, Faculty of Mathematics and Physics, Department of Macromolecular Physics,
V Holešovičkách 2, CZ-18000 Praha 8, Czech Republic*

In Sec. I of this Supplemental Material, we discuss Langevin equations for the particle motion and the methods used to solve them numerically. Section II gives a detailed derivation of the soliton potential and Sec. III describes the effective single-particle dynamics reflecting the soliton motion. The particle size dependence of barriers ΔU_{sp} for solitary wave propagation is exemplified in Sec. IV for the parameters in Fig. 2 of the main text. In Sec. V, we explain how to calculate diagrams of phase-locked current modes $J_{p,q}$.

I. LANGEVIN EQUATIONS AND METHODS OF THEIR NUMERICAL SOLUTION

Overdamped Brownian motion of N hard spheres of diameter σ in the sinusoidal potential

$$U(x) = \frac{U_0}{2} \cos\left(\frac{2\pi x}{\lambda}\right) \quad (\text{S1})$$

driven by the time-periodic force

$$F(t) = F_{\text{dc}} + F_{\text{ac}} \sin\left(\frac{2\pi t}{\tau}\right) \quad (\text{S2})$$

is described by the Langevin equations

$$\frac{dx_i}{dt} = \mu \left[F(t) - \frac{dU}{dx_i} \right] + \sqrt{2D} \eta_i(t), \quad i = 1, \dots, N, \quad (\text{S3})$$

where μ is the mobility, $D = k_{\text{B}}T\mu$, and T the temperature. The $\eta_i(t)$ are stationary Gaussian processes with mean $\langle \eta_i(t) \rangle = 0$ and correlation functions $\langle \eta_i(t)\eta_j(t') \rangle = \delta_{ij}\delta(t-t')$. Periodic boundary conditions are applied for a system with L/λ potential wells. The hard-sphere interaction implies

$$|x_i - x_j| \geq \sigma. \quad (\text{S4})$$

Results presented in the main text were obtained by numerical integration of Langevin equations (S3) under consideration of the hard-sphere constraint (S4), using the recently developed Brownian cluster dynamics algorithm [40, 41] with time step $\Delta t = 10^{-4}\lambda^2/\mu U_0$. We checked these results against Brownian dynamics simulations, where the hard-sphere interaction is treated based on elastic collision schemes [42, 43].

In our numerical treatment, we rescaled quantities to dimensionless variables by taking λ , U_0 , and $\lambda^2/\mu U_0$ as units of length, energy, and time, respectively. All quantities were sampled after a transient time, where the system was brought into a stationary state.

Particle currents in the stationary states were obtained by taking averages of the instantaneous values

$$J(t) = \frac{1}{L} \sum_{i=1}^N \frac{dx_i}{dt}. \quad (\text{S5})$$

The instantaneous velocities $v_i(t) = dx_i(t)/dt$ in Eq. (S5) were calculated by taking difference quotients $[x_i(t + \Delta t) - x_i(t)]/\Delta t$. The currents J shown in Figs. 2(a), 2(b), and 4(c), 4(d) are the time-averaged instantaneous currents $J(t)$ in the steady state, i.e. $J = \int_0^{M\tau} dt J(t)/M\tau$ with $M \gg 1$.

II. SOLITON POTENTIAL

For modeling the soliton dynamics in a single-particle description, we determine the time-averaged mean forces acting on the clusters involved in the wave propagation. These clusters are the core soliton cluster of size n_c and the composite soliton cluster of size $n_b + n_c$, see Figs. 3 and S1.

The time-averaged force acting on a single particle at position x is

$$\bar{F}(x) = F_{\text{dc}} - \frac{dU(x)}{dx}. \quad (\text{S6})$$

In an n -cluster, particles keep in touch at positions $x_1(t)$, $x_2(t) = x_1(t) + \sigma, \dots$, $x_n(t) = x_1(t) + (n-1)\sigma$. The center of mass velocity of such n -cluster is given by the mean external force

$$\bar{F}_n(x_1) = \frac{1}{n} [\bar{F}(x_1) + \dots + \bar{F}(x_n)] \quad (\text{S7})$$

acting on the n -cluster. We have defined the position of the n -cluster to be the position x_1 of the leftmost particle in the n -cluster.

The force \bar{F}_n can be written as

$$\bar{F}_n(x) = F_{\text{dc}} - \frac{d}{dx} U_n(x), \quad (\text{S8})$$

where $U_n(x)$ is the potential of an n -cluster given after Eq. (3) in the main text:

$$U_n(x) = \frac{1}{n} \sum_{i=0}^{n-1} U(x + i\sigma). \quad (\text{S9})$$

As discussed in the main text and illustrated in Figs. 3 and S1, we can describe one period of soliton propagation as follows: Initially, a core soliton cluster of size n_c detaches from a composite cluster at a position x_{det}^+ . The plus in the superscript indicates that it is the position of the core cluster (soliton) *right after* its detachment. Right before the detachment, the soliton position is that of the composite cluster, i.e. $x_{\text{det}}^+ - n_b\sigma$. In the time after the detachment, the n_c -cluster propagates until attaching to an n_b -cluster at position x_{att} . Due to the attachment, a composite cluster of size $n_b + n_c$ forms. The soliton position at the moment of attachment is x_{att} and thereafter it is the position of the moving composite cluster. The motion of the newly formed composite cluster continues until it reaches position

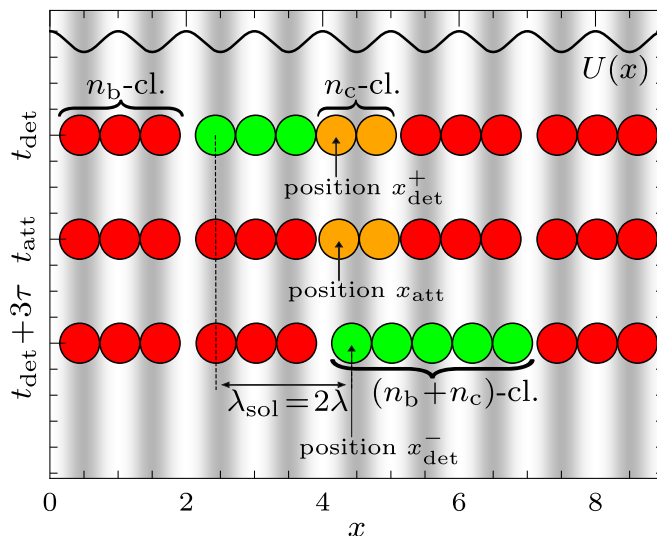


FIG. S1. Soliton propagation from Fig. 3 of the main text, where the positions x_{det}^+ , x_{att} , and x_{det}^- of the soliton are indicated. The position x_{det}^+ is that of the core soliton n_c -cluster right after its detachment from a composite cluster, x_{att} is the position, when the core n_c -cluster attaches to an n_b -cluster, and x_{det}^- is the position of the composite $(n_b + n_c)$ -cluster right before the detachment of a new core n_c -cluster.

x_{det}^- . At this moment, the process starts anew, i.e. a core n_c -cluster detaches from the composite cluster at position $x_{\text{det}}^- + n_b\sigma$. In each detachment event of a core n_c -cluster, the soliton position jumps by $n_b\sigma$.

The soliton potential describes the continuous soliton motion in the interval $[x_{\text{det}}^+, x_{\text{det}}^-]$, which is given by the cluster potential $U_{n_c}(x)$ in the subinterval $[x_{\text{det}}^+, x_{\text{att}}]$ and by the cluster potential $U_{n_b+n_c}(x)$ in the subinterval $[x_{\text{att}}, x_{\text{det}}^-]$:

$$U_{\text{sol}}(x) = \begin{cases} U_{n_c}(x) + C, & x_{\text{det}}^+ \leq x \leq x_{\text{att}}, \\ U_{n_b+n_c}(x), & x_{\text{att}} \leq x \leq x_{\text{det}}^-. \end{cases} \quad (\text{S10})$$

This is Eq. (3) of the main text, where the constant $C = U_{n_b+n_c}(x_{\text{att}}) - U_{n_c}(x_{\text{att}})$ is added to $U_{n_c}(x)$ for making $U_{\text{sol}}(x)$ continuous at x_{att} . The length $x_{\text{det}}^- - x_{\text{det}}^+$ of the continuous soliton motion gives the wavelength λ_{sp} of the associated single-particle potential $U_{\text{sp}}(x)$ in Eq. (S11) below.

While thermal noise is neglected in the construction of the soliton potential, it is considered in the single-particle description of the soliton dynamics, see Eq. (S14) below.

III. SINGLE-PARTICLE DESCRIPTION OF SOLITON DYNAMICS

The single-particle potential $U_{\text{sp}}(x)$ obtained by stitching copies of the soliton potential $U_{\text{sol}}(x)$ in Eq. (S10) and Eq. (3) of the main text is

$$U_{\text{sp}}(x) = \sum_{j=-\infty}^{\infty} I_j(x) [U_{\text{sol}}(x - j\lambda_{\text{sp}}) - j\Delta U_{\text{sol}}], \quad (\text{S11})$$

where $\lambda_{\text{sp}} = x_{\text{det}}^- - x_{\text{det}}^+$, see Fig. S1,

$$\Delta U_{\text{sol}} = \lim_{\varepsilon \rightarrow 0^+} [U_{\text{sol}}(x_{\text{det}}^+ + \varepsilon) - U_{\text{sol}}(x_{\text{det}}^- - \varepsilon)] , \quad (\text{S12})$$

and $I_j(x)$ is the indicator function for the interval $[x_{\text{det}}^+ + j\lambda_{\text{sp}}, x_{\text{det}}^- + j\lambda_{\text{sp}}[$,

$$I_j(x) = \begin{cases} 1, & \text{for } x \in [x_{\text{det}}^+ + j\lambda_{\text{sp}}, x_{\text{det}}^- + j\lambda_{\text{sp}}[, \\ 0, & \text{otherwise.} \end{cases} \quad (\text{S13})$$

The overdamped Brownian motion of a single particle in the potential $U_{\text{sp}}(x)$ driven by $F(t)$ is described by the Langevin equation

$$\frac{dx}{dt} = \mu \left[F(t) - \frac{dU_{\text{sp}}}{dx} \right] + \sqrt{2D(x)} \eta(t) , \quad (\text{S14})$$

where $\eta(t)$ is a stationary Gaussian process with $\langle \eta(t) \rangle = 0$, $\langle \eta(t)\eta(t') \rangle = \delta(t - t')$, and $D(x)$ is a space-dependent diffusion coefficient

$$D(x) = \frac{D}{n(x)} , \quad (\text{S15})$$

with

$$n(x) = \begin{cases} n_c , & \text{for } x \in [x_{\text{det}}^+ + j\lambda_{\text{sp}}, x_{\text{att}} + j\lambda_{\text{sp}}[, j \in \mathbb{Z} , \\ n_b + n_c , & \text{otherwise.} \end{cases} \quad (\text{S16})$$

The Langevin equation (S14) is in Ito interpretation.

IV. DEPENDENCE OF BARRIERS ΔU_{sp} ON PARTICLE SIZE

Single-particle potentials $U_{\text{sp}}(x)$ at $F_{\text{dc}} = 1$ are displayed in Fig. S2 for (a) $\sigma = 0.4\lambda$ and (b) $\sigma = 0.5\lambda$. For $\sigma = 0.4\lambda$, $U_{\text{sp}}(x)$ has pronounced barriers ΔU_{sp} , giving rise to the robust phase-locking in Fig. 2 of the main text, which remains largely observable in the presence of thermal noise.

How ΔU_{sp} depends on the particle diameter σ is shown in Fig. S3 for the system in Fig. 2 with $L/\lambda = 20$ potential wells and $N = 21$ particles. The ΔU_{sp} are much smaller than U_0 and run through maxima between zero points occurring at magic diameters $\sigma = \lambda(n - 1)/n$, $n = 2, 3, \dots$ [30]. With increasing σ , the maxima of ΔU_{sp} decrease, making small diameters favorable for studies of phase-locking in the presence of thermal noise. For $\sigma = 0.4\lambda$ in Fig. 2, ΔU_{sp} is about $0.18U_0$, which is sufficient to obtain phase-locked currents for $k_{\text{B}}T = 0.01U_0$.

A comparison of the many-particle currents in Fig. 2(b) with those obtained from single-particle simulations is shown in the inset of Fig. S3. In the zero-noise limit, the single-particle results agree well with the many-particle data, as in Fig. 4(d) of the main text. For $k_{\text{B}}T = 0.01U_0$, the widths of frequency intervals, where phase-locked values $J_{p,q}$ manifest themselves as slopes in the curves are nearly the same. Interestingly, the currents obtained from single-particle modeling are slightly shifted to smaller frequencies and smaller current values, an effect related to the

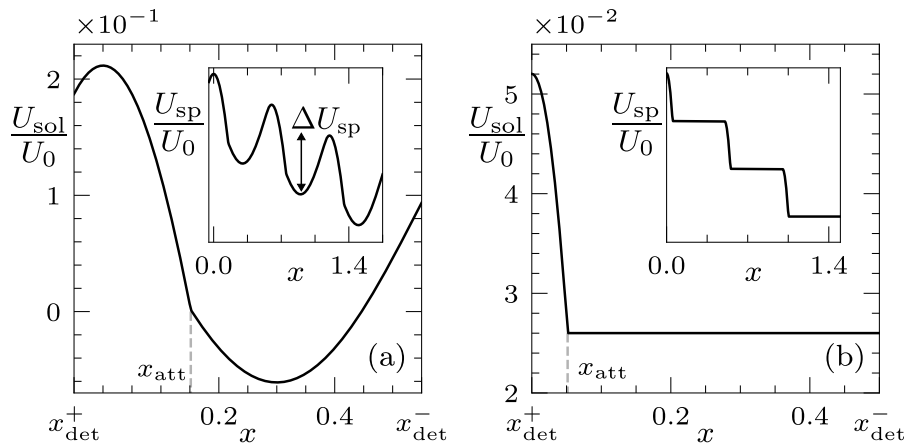


FIG. S2. Single-particle potentials [Eq. (S11)] at $F_{\text{dc}} = 1$ for (a) $\sigma = 0.4\lambda$ and (b) $\sigma = 0.5\lambda$.

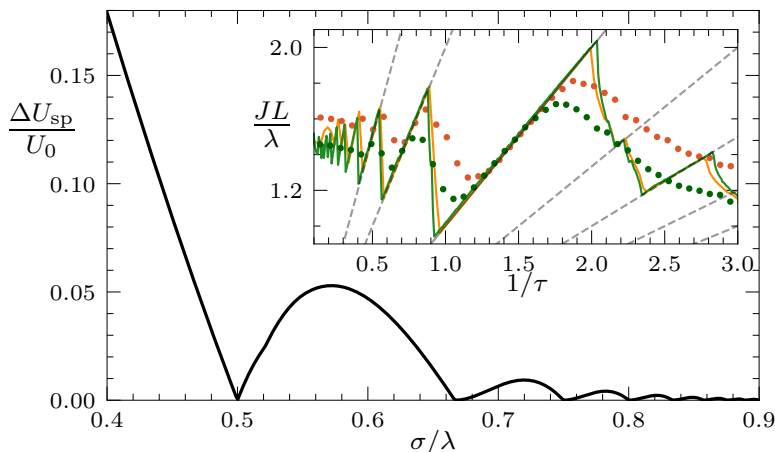


FIG. S3. Variation of barriers ΔU_{sp} of the single-particle potential with the particle diameter σ for the system in Fig. 2 of the main text. The inset shows the many-particle currents from Fig. 2(b) ($\sigma = 0.4\lambda$, orange) in comparison with currents calculated from single-particle simulations (green) in the potential U_{sp} . Lines mark the results in the zero-noise limit and symbols for thermal noise at $k_{\text{B}}T/U_0 = 0.01$.

construction of $U_{\text{sp}}(x)$ in the zero-noise limit.

V. DIAGRAM OF PHASE-LOCKED MODES

Knowing $U_{\text{sp}}(x)$ with wavelength λ_{sp} , we can predict the parameter intervals, where specific phase-locked modes p/q occur. Starting point is the construction of the one-period propagator $G(x; \Gamma)$ for the single-particle dynamics according to Eq. (S14) in the absence of noise [$D(x) = 0$]. This propagator depends on the set of driving parameters $\Gamma = (F_{\text{dc}}, F_{\text{ac}}, \tau)$ and gives the final position $x_f = G(x; \Gamma)$ after one period τ of the driving, if the particle starts at the initial position x . For brevity, we suppress the argument Γ in the propagator in the following.

For a phase-locked periodic mode with value q , the particle must be at an equivalent position in the periodic potential after q periods of the driving, i.e. the difference between the final position $x_f^{(q)}$ after the q periods and the

initial position x must be an integer multiple of λ_{sp} . The final position $x_f^{(q)}$ is given by the q -period propagator $G^{(q)}(x)$, which is obtained by q -fold composition of the one-period propagator:

$$x_f^{(q)}(x) = G^{(q)}(x) = \underbrace{G \circ \dots \circ G(x)}_{q \text{ times}}. \quad (\text{S17})$$

The smallest q for which there exists an $x_* \in [0, \lambda_{\text{sp}}[$, where $x_f^{(q)}(x_*) - x_*$ is an integer multiple of λ_{sp} , is the q of a phase-locked mode. The q of such a mode satisfies

$$[G^{(q)}(x_*) \bmod \lambda_{\text{sp}}] - x_* = 0, \quad (\text{S18})$$

where $[a \bmod b] \in [0, b[$ is the remainder when a is divided by b . The number p of wavelengths λ_{sp} by which the particle is displaced after q periods of the driving is

$$p = \frac{|G^{(q)}(x_*) - x_*|}{\lambda_{\text{sp}}}. \quad (\text{S19})$$

Equations (S18) and (S19) determine q and p values of a phase locked mode.

A fixed point x_* of $[G^{(q)}(x) \bmod \lambda_{\text{sp}}]$ in Eq. (S18) corresponds to a limit cycle of $[G^{(1)}(x) \bmod \lambda_{\text{sp}}]$ that runs through q points. Each of these points is a fixed point x_* of $[G^{(q)}(x) \bmod \lambda_{\text{sp}}]$, i.e. if there is one fixed point x_* according to Eq. (S18), there will be $q-1$ further fixed points belonging to the same limit cycle and satisfying Eq. (S18). A fixed point x_* is stable against small perturbations if $|\partial_x G^{(q)}(x_*)| < 1$ [44]. Unstable fixed points are excluded from the analysis. In the numerical procedure described next for determining p/q , we moreover checked for 20 sets of driving parameters Γ that the attraction basin of the fixed points covers the whole interval $x \in [0, \lambda_{\text{sp}}[$: for each Γ , iteratively mapping of 100 randomly chosen initial positions $x \in [0, \lambda_{\text{sp}}[$ always converged to same limit cycle.

In the numerical procedure, we search for zeros of $H^{(q)}(x) = [G^{(q)}(x) \bmod \lambda_{\text{sp}}] - x$ in $[0, \lambda_{\text{sp}}[$, i.e. fixed points of $[G^{(q)}(x) \bmod \lambda_{\text{sp}}]$. Starting with $q = 1$, q is incremented by one until a root is found. This gives the q of the phase-locked mode.

To determine the zeros of $H^{(q)}(x)$, we divide the interval $[0, \lambda_{\text{sp}}[$ into $M = 50$ equidistant points x_i , $i = 1, \dots, M$, and identify all successive points x_i and x_{i+1} , where $H^{(q)}(x)$ changes sign. There can be several of such pairs, i.e. we obtain a list of intervals $[x_i^{(\alpha)}, x_{i+1}^{(\alpha)}]$, $\alpha = 1, \dots, m < M$. Applying the Van Wijngaarden–Dekker–Brent method [45] on each of these intervals, the points $x_0^{(\alpha)}$ of sign change in all intervals α are determined with high accuracy of 11 significant digits. Not all $x_0^{(\alpha)}$ are roots of Eq. (S18), because $H^{(q)}(x)$ can have a jump at $x_0^{(\alpha)}$, i.e. $|H^{(q)}(x_0^{(\alpha)} - 0) - H^{(q)}(x_0^{(\alpha)} + 0)| > 0$. In the procedure, we chose $|H^{(q)}(x_0^{(\alpha)} - \delta) - H^{(q)}(x_0^{(\alpha)} + \delta)| > \epsilon$ with $\delta = 10^{-6}$ and $\epsilon = 10^{-3}$ as criterion for excluding $x_0^{(\alpha)}$ as roots of Eq. (S18).

Using this method, we can scan the parameter space of the driving and determine for each Γ which mode p/q of phase-locked many-particle current occurs. This in particular reveals the parameter region where a certain mode appears. We found very good agreement with simulated data. As a demonstration, we show in Fig. S4 the diagram of phase-locked current modes in dependence of $1/\tau$ and F_{dc} for particle diameter $\sigma = 0.4\lambda$ at fixed amplitude $F_{\text{ac}} = 1.5$ of the time-periodic driving. Modes are shown up to $q = 5$. Areas of $1/\tau$ and F_{dc} values marked in white color contain either phase-locked modes with $q > 5$ or points, where aperiodic nonsynchronized dynamics occurs.

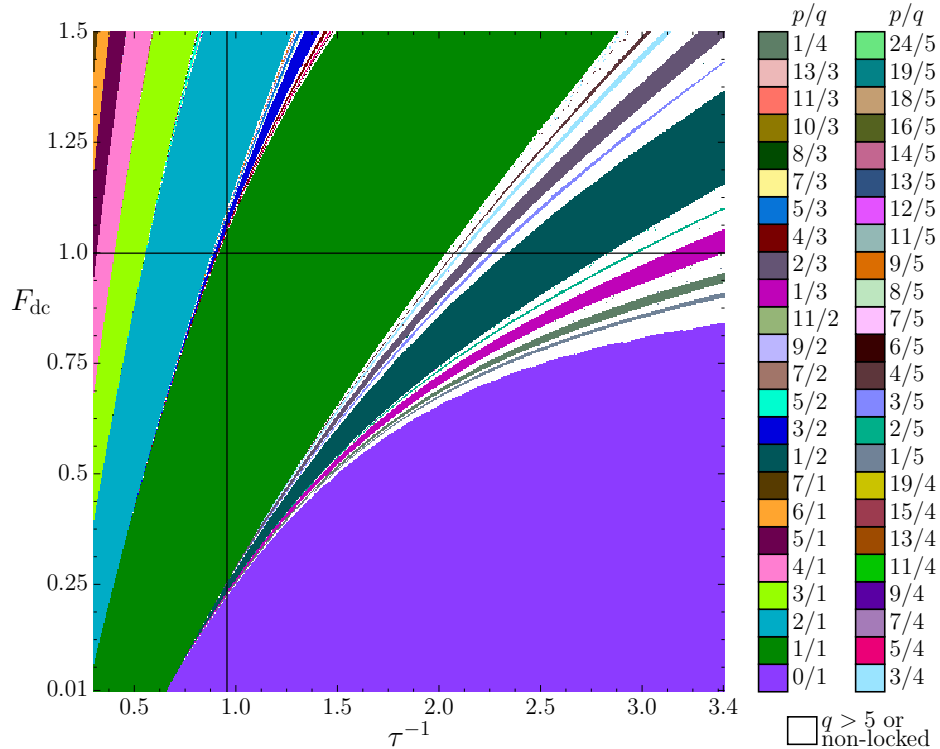


FIG. S4. Diagram of p/q values specifying phase-locked many-particle currents $J_{p,q}$ for hard-sphere diameter $\sigma = 0.4\lambda$ in dependence of $1/\tau$ and F_{dc} for fixed amplitude $F_{ac} = 1.5$ of the time periodic driving. The data were calculated from Eqs. (S18) and (S19) with the numerical procedure described after Eq. (S19). Parameter regions, where modes with $q > 5$ can occur, as well as aperiodic states not synchronized with the driving, are colored in white. Following the vertical black line in the diagram gives the phase-locked modes of currents in the zero-noise limit shown in Fig. 2(a) of the main text (variation of F_{dc} at fixed $F_{ac} = 1.5$ and $1/\tau = 3/\pi$). Following the horizontal black line in the diagram gives the phase-locked modes of currents in the zero-noise limit shown in Fig. 2(b) of the main text (variation of $1/\tau$ at fixed $F_{dc} = 1$ and $F_{ac} = 1.5$).

When following the black horizontal line at fixed $F_{dc} = 1$ in Fig. S4, we can infer the phase-locked current modes shown in Fig. 2(b) of the main text for $\sigma = 0.4\lambda$ (variation of $1/\tau$ at fixed $F_{dc} = 1$ and $F_{ac} = 1.5$). For example, the integer Shapiro steps at phase-locked currents $J_{p,q} = (p/q)\lambda/L\tau$ with $p/q = 2/1$ and $p/q = 1/1$ appear for $1/\tau$ in the intervals 0.56-0.87 and 0.92-2.03 in Fig. S4, as can be inferred from the intervals where the horizontal black line runs through the areas marked in turquoise-blue and green. This is in excellent agreement with the intervals of $1/\tau$, where the corresponding phase-locked current modes appear in Fig. 2(b). Likewise, the intervals $1/\tau$, where the fractional Shapiro steps with $p/q = 2/3$, $1/2$, $2/5$, and $1/3$ appear in Fig. 2(b) are correctly predicted by the mode diagram in Fig. S4, see the intervals, where the horizontal black line runs through respective colored areas.

When following the black vertical line at fixed $1/\tau = 3/\pi$ in Fig. S4, we can infer the phase-locked current modes shown in Fig. 2(a) of the main text for $\sigma = 0.4\lambda$ (variation of F_{dc} at fixed $F_{ac} = 1.5$ and $1/\tau = 3/\pi$). Comparing the appearance of predicted phase-locked currents in Fig. 2(a) with the predicted one from Fig. S4, we again find excellent agreement.